LIGO-P080051-02-Z
AEI-2008-043

Parameter-space correlations of the optimal statistic for continuous gravitational-wave detection

Holger J. Pletsch*
Max-Planck-Institut für Gravitationsphysik (Albert-Einstein-Institut) and Leibniz Universität Hannover, Callinstr. 38, 30167 Hannover, Germany

The phase parameters of matched-filtering searches for continuous gravitational-wave signals are sky position, frequency and frequency time-derivatives. The space of these parameters features strong global correlations in the optimal detection statistic. For observation times smaller than one year, the orbital motion of the Earth leads to a family of global-correlation equations which describes the "global maximum structure" of the detection statistic. The solution to each of these equations is a different hypersurface in parameter space. The expected detection statistic is maximal at the intersection of these hypersurfaces. The global maximum structure of the detection statistic from stationary instrumental-noise artifacts is also described by the global-correlation equations. This permits the construction of a veto method which excludes false candidate events.

PACS numbers: 04.80.Nn, 95.55.Ym, 95.75.-z, 97.60.Gb

I. INTRODUCTION

The emission of continuous gravitational waves (CW) is expected, for instance, from spinning neutron stars with non-axisymmetric deformations. If the system is isolated, it is losing angular momentum through radiation and is slowing down. Therefore the gravitational-wave frequency would be slowly decreasing for this long-lasting type of signal. Such CW sources are among the primary targets of Earth-based, laser-interferometric and resonant-bar detectors.

The terrestrial location of the detectors generates a Doppler modulation of the signal caused by the detector's motion relative to the solar system barycenter (SSB). The observed phase therefore depends on "phase parameters", which describe the intrinsic frequency evolution and the source's sky location. In addition, there is a time-varying amplitude modulation due to the antenna patterns changing with the Earth's spinning motion. The latter variations depend on the "amplitude parameters", which are the two polarization amplitudes, and the polarization angle of the gravitational wave.

To extract CW signals buried in the detector noise, the optimal data analysis scheme is derived in [1] based on the principle of maximum likelihood detection leading to coherent matched filtering. It is shown, that the amplitude parameters together with the initial-phase parameter can be eliminated by analytically maximizing the detection statistic, such that the search space is just the phase parameters: sky position, frequency and frequency time-derivatives. This detection statistic is commonly referred to as the $\mathcal{F}$-statistic. For a given sequence of data, wide-band all-sky searches evaluate the $\mathcal{F}$-statistic over a large number of template-grid points in parameter space. The parameters of the templates for which a predetermined threshold is exceeded are registered as candidate events for potential gravitational-wave signals.

In the *local* parameter-space neighborhood of a given signal one can define a metric [2, 3, 4] from the fractional loss in expected $\mathcal{F}$-statistic. This fractional loss defines the dimensionless "mismatch" μ. Let λ define a vector of phase parameters for a template. If $\lambda_{\rm S}$ denotes the signal's phase parameters, then the metric $g_{ij}(\lambda_{\rm S})$ is obtained by Taylor-expanding the mismatch at $\lambda_{\rm S}$ with respect to the small parameter offsets $\Delta\lambda \equiv \lambda_{\rm S} - \lambda$ to quadratic order: $\mu = \sum_{ij}\ g_{ij}(\lambda_{\rm S})\ \Delta\lambda^i\Delta\lambda^j + \mathcal{O}[(\Delta\lambda)^3]$.

This work identifies the *global* parameter-space regions where the detection statistic $\mathcal{F}$ is expected to have large values close to maximal without restriction to the local neighborhood of the signal location. In this paper, these regions are referred to as the "*global large-value structure*". To find the global large-value structure of the $\mathcal{F}$-statistic, a simplified detection statistic $\mathcal{F}^\star$ (approximating $\mathcal{F}$) is considered. The locations in parameter space where $\mathcal{F}^\star$ is expected to be maximal are referred to as the "*global maximum structure*". For increasing parameter offsets from the given signal's parameters this global maximum structure of $\mathcal{F}^\star$ (and therefore also the global large-value structure of $\mathcal{F}$) is found to become significantly different from local approximation obtained from the metric.

A previous study [5] examined monochromatic signals in the restricted phase-parameter space of sky location and frequency. It was shown that in some different approximate detection statistic, such signals can generate "circles in the sky" while searching a range of template frequencies. The collection of these circles forms a two-dimensional hypersurface in the three-dimensional parameter space, described by a single equation. Here, even in this restricted parameter space, this hypersurface is only an approximation of the description of the global maximum structure of the $\mathcal{F}^\star$-statistic to first order in observation time T.

The present work shows that the global maximum structure of the detection statistic $\mathcal{F}^\star$ is described by

*Electronic address: Holger.Pletsch@aei.mpg.de

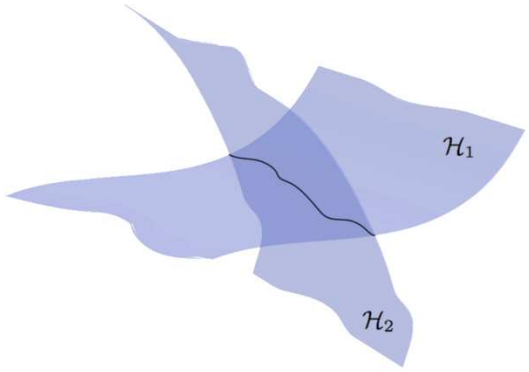

FIG. 1: Schematic drawing of intersection of two representative global-correlation hypersurfaces $\mathcal{H}_1$ and $\mathcal{H}_2$. The region of intersection, shown by the solid black curve, describes the global maximum structure of the simplified detection statistic $\mathcal{F}^\star$, because the expectation value of $\mathcal{F}^\star$ is maximal in these locations. For illustration purposes only two hypersurfaces are shown, whereas in general one might need to consider more hypersurfaces.

a separate equation for each order of T. The solution to each of these equations is a different hypersurface in parameter space. Therefore, it is this family of *global-correlation hypersurfaces*, which describes the global maximum structure of $\mathcal{F}^\star$: The detection statistic $\mathcal{F}^\star$ is expected to be maximal at the intersection of these hypersurfaces. This idea is illustrated schematically in Figure 1. The same results also apply when considering the generalization to non-monochromatic signals allowing for an intrinsic frequency evolution of the source.

This paper is organized as follows. Section II briefly reviews the matched-filtering method for CW sources. Section III describes an approximate signal model which leads to the simplified detection statistic allowing the analytical exploration of its global maximum structure. Section IV presents the global-correlation equations of the phase-parameter space and illustrates the geometry of the global-correlation hypersurfaces. In addition, the search-parameter regions are derived for which the approximations used are valid. In Section V the predictions made by the global-correlation hypersurfaces are compared to a fully coherent $\mathcal{F}$-statistic search in data sets of software-simulated sources with no detector noise as well as of hardware-injected CW signals in the presence of real detector noise. In Section VI the global large-value of the detection statistic which is caused by stationary instrumental-noise artifacts mimicking astrophysical sources is found to be also well described by the global-correlation equations, and thus a veto method is constructed. Section VII discusses the effects of the Earth's spinning motion in the context of the present topic. Finally a concluding section follows.

II. OPTIMAL FILTERING FOR CONTINUOUS GRAVITATIONAL-WAVE SIGNALS

In the absence of any signal, the detector output data time series $x(t)$ at detector time t only contains noise $n(t)$, which is assumed to be a zero-mean, stationary and Gaussian random process. If a signal $h(t)$ is present, the noise is assumed to be additive, $x(t) = n(t) + h(t)$. Denote by t_{SSB} the time measured at the solar system barycenter. For a detector at fixed position and orientation, at the SSB the continuous gravitational-wave signal is described by a sinusoid of constant amplitude and a phase given by

$$\Psi(t_{\mathrm{SSB}}) = \Phi_0 + \Phi(t_{\mathrm{SSB}}) = \Phi_0 + 2\pi \sum_{k=0}^{\infty} \frac{f^{(k)}}{(k+1)!}\, t_{\mathrm{SSB}}^{k+1}, \quad (1)$$

where Φ_0 is the initial phase, $f^{(0)} \equiv f$ denotes the frequency, and $f^{(k>0)}$ the k'th frequency time-derivative, defining every parameter $f^{(k)}$ at $t = 0$ at the SSB. The integer $s > 0$ denotes the number of frequency time-derivatives to be taken into account, therefore it is set $f^{(k>s)} = 0$. In the case of an isolated rapidly rotating neutron star with non-axisymmetric deformations and negligible proper motion [6], the waveforms corresponding to the plus (+) and cross (×) polarizations are

$$h_+(t) = A_+ \sin\Psi(t), \qquad h_\times(t) = A_\times \cos\Psi(t). \quad (2)$$

The Earth's motion with respect to the SSB leads to Doppler effects causing amplitude and phase modulations of the CW signal received at the detector. Define $\mathbf{n}$ as the constant unit vector pointing from the SSB to the source. Neglecting relativistic and higher order corrections, a wavefront arriving at the detector at time t, passes the SSB at time

$$t_{\mathrm{SSB}} = t + \frac{\mathbf{r}(t)\cdot\mathbf{n}}{c}\,, \quad (3)$$

where the vector $\mathbf{r}(t)$ connects from the SSB to the detector, and c is the speed of light.

It is shown in [1] that the resulting phase evolution of the continuous gravitational-wave signal can be reproduced without significant loss in signal-to-noise ratio by the model

$$\Phi(t) = 2\pi \sum_{k=0}^{s} \left[\frac{f^{(k)}\, t^{k+1}}{(k+1)!} + \frac{\mathbf{r}(t)}{c}\cdot\mathbf{n}\, \frac{f^{(k)}\, t^{k}}{k!} \right]. \quad (4)$$

The received signal is also amplitude modulated by the varying antenna-pattern of the detector due to its motion with the rotation of the Earth. The dimensionless signal response function $h(t)$ of an interferometric detector to a weak plane gravitational wave in the long-wavelength approximation is a linear combination of the form:

$$h(t) = F_+(t)\, h_+(t) + F_\times(t)\, h_\times(t), \quad (5)$$

where $F_{+,\times}$ are called the antenna-pattern functions, resulting in the amplitude modulations from Earth's spinning motion. They lie in the range $-1 \leq F_{+,\times} \leq 1$, and depend on the orientation of the detector and source, and on the polarization angle ψ of the waves.

The optimal detection statistic [1, 7] obtained from the likelihood ratio Λ defines the matched filter

$$\ln \Lambda = \frac{T}{S_h}\left[(x||h) - \frac{1}{2}(h||h)\right], \tag{6}$$

where S_h is the one-sided noise strain spectral density which is assumed to be constant over the narrow bandwidth of the signal, and the inner product is defined as

$$(x||y) \equiv \frac{2}{T}\int_{-T/2}^{T/2} x(t)\, y(t)\, \mathrm{d}t, \tag{7}$$

centering the coherent observation-time interval of duration T around $t = 0$. Replacing the amplitude parameters in Equation (6) by their values which maximize $\ln \Lambda$, the so-called maximum likelihood (ML) estimators, defines the detection statistic $\mathcal{F}$ as

$$\mathcal{F} \equiv \ln \Lambda_{\mathrm{ML}}. \tag{8}$$

III. MATCHED-FILTERING DETECTION STATISTIC OF A SIMPLIFIED SIGNAL MODEL

A. The simplified signal model

The phase of the continuous gravitational-wave signal is expected to change very rapidly at the detector site on the Earth over a characteristic time length of typically less than ten seconds, whereas the amplitude of the signal changes with a period of one sidereal day. As a result [8], the detection of a CW signal requires an accurate model of its phase, because even 1/4 of a cycle difference between template and signal can lead to a loss in signal-to-noise ratio of 10%. Whereas modeling of its amplitude is less critical. Therefore, the antenna pattern functions $F_{+,\times}$ are assumed to be constant, so that the signal model (5) becomes

$$h(t) = A_1 \cos\Phi(t) + A_2 \sin\Phi(t)\ , \tag{9}$$

where $A_{1,2}$ are defined to be the constant effective amplitudes. The validity of this approximation is investigated using Monte Carlo simulations in [8].

The vector $\mathbf{r}(t)$ connecting the SSB and the detector can be decomposed into an orbital component $\mathbf{r}_{\mathrm{orb}}(t)$ and a spin component $\mathbf{r}_{\mathrm{spin}}(t)$ as

$$\mathbf{r}(t) = \mathbf{r}_{\mathrm{orb}}(t) + \mathbf{r}_{\mathrm{spin}}(t)\ , \tag{10}$$

where $\mathbf{r}_{\mathrm{orb}}(t)$ represents the vector from the SSB to the Earth's barycenter, and $\mathbf{r}_{\mathrm{spin}}(t)$ is the vector from the Earth's barycenter to the detector. Thus, substituting the decomposition (10) into Equation (4) one can write separately the orbital component $\phi_{\mathrm{orb}}(t)$ and the spin component $\phi_{\mathrm{spin}}(t)$ in the phase model (4) as

$$\Phi(t) = 2\pi\left(\sum_{k=0}^{s}\frac{f^{(k)}}{(k+1)!}\,t^{k+1}\right) + \phi_{\mathrm{orb}}(t) + \phi_{\mathrm{spin}}(t), \tag{11}$$

where

$$\phi_{\mathrm{orb}}(t) \ \equiv\ 2\pi\,\frac{\mathbf{r}_{\mathrm{orb}}(t)\cdot\mathbf{n}}{c}\left(\sum_{k=0}^{s}\frac{f^{(k)}}{k!}t^{k}\right), \tag{12}$$

$$\phi_{\mathrm{spin}}(t) \ \equiv\ 2\pi\,\frac{\mathbf{r}_{\mathrm{spin}}(t)\cdot\mathbf{n}}{c}\left(\sum_{k=0}^{s}\frac{f^{(k)}}{k!}t^{k}\right). \tag{13}$$

The orbital motion of the Earth has a period of one year, so its angular frequency is $\Omega_{\mathrm{orb}} = 2\pi/1\,\mathrm{yr}$. Fully coherent all-sky searches for observation times T much larger than a few days are computationally prohibitive [1, 3]. Thus for computationally feasible coherent searches or coherent stages of hierarchical multistage searches [9, 10] the typical observation time baseline would be of order a few days. Therefore, only observation times T are considered, which are much shorter than one year: $\Omega_{\mathrm{orb}}T \ll 2\pi$. Then the component $\mathbf{r}_{\mathrm{orb}}(t)$ will vary slowly and one may use a Taylor expansion at time t_0 with

$$\mathbf{r}_{\mathrm{orb}}(t) = \sum_{\ell=0}^{\infty}\mathbf{r}_{\mathrm{orb}}^{(\ell)}(t_0)\,\frac{(t-t_0)^{\ell}}{\ell!}, \tag{14}$$

where $\mathbf{r}_{\mathrm{orb}}^{(\ell)}(t_0)$ denotes the ℓ'th derivative with respect to time of $\mathbf{r}_{\mathrm{orb}}(t)$ evaluated at t_0. Without loss of generality we may choose $t_0 = 0$ as the midpoint of the observation of duration T in the following discussion. Define $\boldsymbol{\xi} \equiv \mathbf{r}_{\mathrm{orb}}(0)/c$ with $\xi \equiv |\boldsymbol{\xi}|$ such that

$$\boldsymbol{\xi}^{(\ell)} = \frac{\mathbf{r}_{\mathrm{orb}}^{(\ell)}(0)}{c} \qquad \text{and} \qquad \xi^{(\ell)} = \left|\boldsymbol{\xi}^{(\ell)}\right|. \tag{15}$$

Together with Equation (14) the orbital component of the phase (12) can be written as

$$\begin{aligned}\phi_{\mathrm{orb}}(t) \ &=\ 2\pi\left(\sum_{k=0}^{s}f^{(k)}\frac{t^{k}}{k!}\right)\left(\sum_{\ell=0}^{\infty}\frac{t^{\ell}}{\ell!}\,\boldsymbol{\xi}^{(\ell)}\cdot\mathbf{n}\right)\\ &=\ 2\pi\left[\sum_{k=0}^{\infty}t^{k}\left(\sum_{\ell=0}^{k}\frac{f^{(\ell)}\,\boldsymbol{\xi}^{(k-\ell)}\cdot\mathbf{n}}{\ell!\,(k-\ell)!}\right)\right].\end{aligned} \tag{16}$$

The spinning motion of the Earth has a period of one sidereal day (1 sd), which translates into an angular frequency of $\Omega_{\mathrm{spin}} = 2\pi/1\,\mathrm{sd}$. The corresponding average velocity of $v_{\mathrm{spin}}/c \approx 10^{-6}$ is two orders of magnitude smaller than the corresponding orbital velocity, $v_{\mathrm{orb}}/c \approx 10^{-4}$. In what follows we neglect the contribution of the spin component $\phi_{\mathrm{spin}}(t)$ to the phase (11). Section VII will discuss in detail the effects of the spin component $\phi_{\mathrm{spin}}(t)$ in terms of the matched-filtering amplitude.

Using $\phi_{\rm orb}(t)$ in the form of Equation (16), we refer to $\Phi_{\rm orb}(t)$ as the "orbital phase model":

$$\Phi_{\rm orb}(t) \equiv 2\pi\left[f\,\boldsymbol{\xi}\cdot\mathbf{n} + \sum_{k=0}^{\infty} t^{k+1}\left(\frac{f^{(k)}}{(k+1)!} + \sum_{\ell=0}^{k+1}\frac{f^{(\ell)}}{\ell!(k-\ell+1)!}\,\boldsymbol{\xi}^{\,(k-\ell+1)}\cdot\mathbf{n}\right)\right]. \quad (17)$$

By reparameterization the orbital phase model (17) can be written as

$$\Phi_{\rm orb}(t) = \sum_{m=0}^{\infty} u_m\, t^m, \quad (18)$$

where the coefficients u_m of the power series are defined by

$$u_0 \equiv 2\pi f\,\boldsymbol{\xi}\cdot\mathbf{n}, \quad (19a)$$

$$u_1 \equiv 2\pi\left(f + f\,\boldsymbol{\xi}^{\,(1)}\cdot\mathbf{n} + f^{(1)}\,\boldsymbol{\xi}\cdot\mathbf{n}\right), \quad (19b)$$

$$u_2 \equiv 2\pi\left(\frac{f^{(1)}}{2} + \frac{f}{2}\,\boldsymbol{\xi}^{\,(2)}\cdot\mathbf{n} + f^{(1)}\,\boldsymbol{\xi}^{\,(1)}\cdot\mathbf{n} + \frac{f^{(2)}}{2}\,\boldsymbol{\xi}\cdot\mathbf{n}\right), \quad (19c)$$

$$u_3 \equiv 2\pi\left(\frac{f^{(2)}}{6} + \frac{f}{6}\,\boldsymbol{\xi}^{\,(3)}\cdot\mathbf{n} + \frac{f^{(1)}}{2}\,\boldsymbol{\xi}^{\,(2)}\cdot\mathbf{n} + \frac{f^{(2)}}{2}\,\boldsymbol{\xi}^{\,(1)}\cdot\mathbf{n} + \frac{f^{(3)}}{6}\,\boldsymbol{\xi}\cdot\mathbf{n}\right), \quad (19d)$$

so that for arbitrary order of $m > 0$ the coefficient u_m is obtained as

$$u_m \equiv 2\pi\left(\frac{f^{(m-1)}}{m!} + \sum_{\ell=0}^{m}\frac{f^{(\ell)}}{\ell!(m-\ell)!}\,\boldsymbol{\xi}^{\,(m-\ell)}\cdot\mathbf{n}\right). \quad (19e)$$

B. The simplified matched-filtering detection statistic

By analogy to Equation (6), we refer to $\ln\Lambda^\star$ as the log likelihood function of the simplified CW signal model described in previous Section III A. Maximization of $\ln\Lambda^\star$ with respect to the unknown amplitudes $A_{1,2}$ yields their ML estimators. By substituting the ML estimators back into $\ln\Lambda^\star$, the simplified detection statistic $\mathcal{F}^\star$ is defined as

$$\mathcal{F}^\star \equiv \ln\Lambda^\star_{\rm ML} = \frac{T}{2\,S_h}\left|(x||\mathrm{e}^{-i\Phi_{\rm orb}})\right|^2 = \frac{T}{2\,S_h}\,|\mathcal{X}|^2, \quad (20)$$

where the detection-statistic amplitude $\mathcal{X}$ has been defined through

$$\mathcal{X} \equiv (x||\mathrm{e}^{-i\Phi_{\rm orb}}), \quad (21)$$

using the orbital phase model $\Phi_{\rm orb}$.

For further simplicity consider a data set $x(t)$ which only contains unit-amplitude signal $\mathrm{s}(t)$, such that

$$x(t) = \Re[\mathrm{s}(t)]. \quad (22)$$

Let the phase-parameter vector $\lambda_{\rm S} = (\{f_{\rm S}^{(k)}\}, \mathbf{n}_{\rm S})$ define the phase $\Phi^{\rm S}_{\rm orb}(t)$ of the signal. Then $\mathrm{s}(t)$ can be expressed as

$$\mathrm{s}(t) = \mathrm{e}^{-i\Phi^{\rm S}_{\rm orb}(t)}, \quad (23)$$

and one obtains $x(t) = \cos\Phi^{\rm S}_{\rm orb}(t)$. The difference in phase $\Delta\Phi_{\rm orb}(t)$ between the phase $\Phi^{\rm S}_{\rm orb}(t)$ of the signal and the phase $\Phi_{\rm orb}(t)$ of a template $\lambda = (\{f^{(k)}\}, \mathbf{n})$ is defined by

$$\Delta\Phi_{\rm orb}(t) \equiv \Phi^{\rm S}_{\rm orb}(t) - \Phi_{\rm orb}(t). \quad (24)$$

The maximization of $\mathcal{F}^\star$ is equivalent to maximizing $|\mathcal{X}|^2$. Using Equation (23) one may rewrite the simplified matched-filtering amplitude $\mathcal{X}$ as

$$\mathcal{X} = \frac{2}{T}\int_{-T/2}^{T/2} x(t)\,\mathrm{e}^{-i\Phi_{\rm orb}(t)}\,\mathrm{d}t = \frac{1}{T}\int_{-T/2}^{T/2}\mathrm{e}^{i\Delta\Phi_{\rm orb}(t)} + \mathrm{e}^{-i\left[\Phi^{\rm S}_{\rm orb}(t)+\Phi_{\rm orb}(t)\right]}\,\mathrm{d}t. \quad (25)$$

Dropping the rapidly oscillating term in Equation (25) yields

$$\mathcal{X} \approx \frac{1}{T}\int_{-T/2}^{T/2}\mathrm{e}^{i\Delta\Phi_{\rm orb}(t)}\,\mathrm{d}t. \quad (26)$$

Thus, Equation (26) shows that $|\mathcal{X}|$ has a global maximum of $|\mathcal{X}| = 1$, if during the observation time interval T the phase difference $\Delta\Phi_{\rm orb}(t)$ is stationary:

$$\frac{\partial\Delta\Phi_{\rm orb}(t)}{\partial t} = 0. \quad (27)$$

Later, we will demonstrate that for the orbital phase model, unity of $|\mathcal{X}|$ can be obtained *not only* for the case where all individual phase parameters exactly match ($\Delta f^{(k)} \equiv f_{\rm S}^{(k)} - f^{(k)} = 0$, $\Delta\mathbf{n} \equiv \mathbf{n}_{\rm S} - \mathbf{n} = \mathbf{0}$) and

so $\Delta\Phi_{\rm orb}(t) = 0$, *but also* for different non-zero offsets ($\Delta f^{(k)} \neq 0, \Delta\mathbf{n} \neq \mathbf{0}$) which compensate each other to achieve $\partial\Delta\Phi_{\rm orb}(t)/\partial t \approx 0$ and thus lead to a value of $|\mathcal{X}|$ close to unity.

IV. GLOBAL-CORRELATION HYPERSURFACES IN PARAMETER SPACE

A. The global-correlation equations

The central goal of this work is to identify those locations in parameter space where the simplified detection statistic $\mathcal{F}^\star$ is maximal, which corresponds to regions where $|\mathcal{X}|^2$ is one. Consistent with Equations (18), (19) and (24), the differences between the coefficients u_m of the template's phase and the coefficients $u_m^{\rm S}$ of the signal's phase are defined by

$$\Delta u_m \equiv u_m^{\rm S} - u_m \,. \tag{28}$$

Thus, Equation (24) can be expressed as

$$\Delta\Phi_{\rm orb}(t) = \sum_{m=0}^{\infty} \Delta u_m \, t^m, \tag{29}$$

and finally one can rewrite Equation (25) as

$$\mathcal{X} = \frac{\mathrm{e}^{i\Delta u_0}}{T} \int_{-T/2}^{T/2} \exp\left(i \sum_{m=1}^{\infty} \Delta u_m \, t^m \right) \mathrm{d}t. \tag{30}$$

It is apparent that $|\mathcal{X}|$ does not depend upon the zero-order term Δu_0, and therefore the same holds for the detection statistic $\mathcal{F}^\star$. The values of Δu_m for which $|\mathcal{X}|$ attains its maximum of $|\mathcal{X}| = 1$ consistent with (27) are obvious from Equation (29), namely when

$$\frac{\partial\Delta\Phi_{\rm orb}(t)}{\partial t} = \sum_{m=0}^{\infty} m \, \Delta u_m \, t^{m-1} = 0, \tag{31}$$

the following central result is obtained: the family of *global-correlation equations* which describes the global maximum structure of $\mathcal{F}^\star$,

$$\Delta u_m = 0, \tag{32}$$

where $m > 0$, because $\mathcal{F}^\star$ is independent of Δu_0. Because $(1, t, t^2, \dots)$ is a basis of the vector space of real polynomials, the zero vector can only be represented by the trivial linear combination, which is given by Equation (32).

Thus, the first global-correlation equation given by $\Delta u_1 = 0$ can be rewritten as

$$f + f\,\boldsymbol{\xi}^{(1)} \cdot \mathbf{n} + f^{(1)}\,\boldsymbol{\xi} \cdot \mathbf{n} = K_1, \tag{33}$$

where $K_1 \equiv u_1^{\rm S}/2\pi$ represents a constant defined by the signal's phase parameters. As a side remark, it should be mentioned that Equation (33) is a generalization of the first-order global-correlation equation found in [5] to signals with non-zero frequency time-derivatives. But in order to describe qualitatively the global maximum structure of the simplified detection statistic in parameter space, considering only the first order (as done in [5]) might not be sufficient. As a matter of fact, this is shown in Section IV D and will be confirmed by analyzing simulated signals later on.

Therefore, continuing to the next order in time, one obtains from the second condition $\Delta u_2 = 0$ the following relation,

$$f^{(1)} + f\,\boldsymbol{\xi}^{(2)} \cdot \mathbf{n} + 2f^{(1)}\,\boldsymbol{\xi}^{(1)} \cdot \mathbf{n} + f^{(2)}\,\boldsymbol{\xi} \cdot \mathbf{n} = K_2, \tag{34}$$

where the constant $K_2 \equiv u_2^{\rm S}/2\pi$ is defined by the signal's phase parameters.

In general, this scheme can extended to arbitrary order $m > 0$. Thus, the family of global-correlation equations represented by $\Delta u_m = 0$ can be written in the form

$$\frac{f^{(m-1)}}{m!} + \sum_{\ell=0}^{m} \frac{f^{(\ell)}\,\boldsymbol{\xi}^{(m-\ell)} \cdot \mathbf{n}}{\ell!(m-\ell)!} = K_m, \tag{35}$$

where the signal's phase parameters determine the constant $K_m \equiv u_m^{\rm S}/2\pi$. In the following the geometry of the solution to the family of equations given by (35) will be explored and the *hypersurfaces* they describe in parameter space will be illustrated.

B. The geometry of the global-correlation equations

Let the space of phase parameters $\lambda = (\{f^{(k)}\}, \mathbf{n})$ be a manifold denoted by $\mathcal{P}$. Previously we defined $\mathbf{n}$ as a unit vector pointing to the source's sky location in the SSB frame of reference. A position on the sky can be determined by two independent coordinates, for example one can use equatorial coordinates of right ascension (RA) and declination, denoted by α and δ, respectively. In these coordinates: $\mathbf{n} = (\cos\delta\,\cos\alpha, \cos\delta\,\sin\alpha, \sin\delta)$. Recall that the integer s is related to the number of spin-down parameters considered ($f^{(k>s)} = 0$), thus the phase-parameter space dimensionality is $s + 3$.

By inspection of Equation (35), it is obvious that for a given continuous gravitational-wave signal the set of solutions to each global-correlation equation $\Delta u_m = 0$, is a *hypersurface* in the search parameter space $\mathcal{P}$. Denoting each hypersurface by $\mathcal{H}_m$ one may write

$$\mathcal{H}_m = \{\lambda \in \mathcal{P} \;:\; \Delta u_m = 0\}, \tag{36}$$

given the signal's phase parameters $u_m^{\rm S}$. The dimensionality of each hypersurface $\mathcal{H}_m$ is $s + 2$.

Using the parameters u_m of Equation (19) define the vector $\mathrm{u} \equiv (\{u_m\}) = (u_1, u_2, \dots)$ and denote the corresponding parameter-space manifold by $\mathcal{U}$. Let the vector $\mathrm{u}^{\rm S} \in \mathcal{U}$ denote the signal's parameters, and define the difference $\Delta\mathrm{u} = \mathrm{u}^{\rm S} - \mathrm{u} = (\Delta u_1, \Delta u_2, \dots)$. Considering

the detection-statistic amplitude $|\mathcal{X}|$ as a function of $\Delta\mathrm{u}$, then this function is extremal with respect to the parameter u_m along the hypersurface $\mathcal{H}_m$ defined by $\Delta u_m = 0$,

$$\left.\frac{\partial\,|\mathcal{X}(\Delta\mathrm{u})|}{\partial u_m}\right|_{\Delta u_m=0} = 0. \tag{37}$$

Obviously, on the intersection of these hypersurfaces $\mathcal{H}_m$ at $\Delta\mathrm{u} = 0$, $|\mathcal{X}|$ is maximum with respect to all the parameters u_m: $\nabla\,|\mathcal{X}(\Delta\mathrm{u}=0)| = 0$. Thus, it follows that the simplified detection statistic $\mathcal{F}^\star$ is also expected to be maximal at the intersection of these hypersurfaces. Therefore, the global maximum structure is defined by the intersection of the global-correlation hypersurfaces $\mathcal{H}_m$. This idea has been shown schematically in Figure 1. In the absence of noise, all candidate events produced by a given CW signal which follows the simplified model introduced in Section III A will be located on the hypersurface $\mathcal{H}_1$, described by Equation (33). From all candidate events located on $\mathcal{H}_1$ those will belong to loudest ones (have largest values of $\mathcal{F}^\star$) which are located at the intersection with hypersurface $\mathcal{H}_2$, which is described by Equation (34). For each higher order m this behavior carries itself forward in the same way.

C. A visualizing example of the global-correlation hypersurfaces

As an illustrative example visualization of the geometrical structure formed by the global-correlation hypersurfaces (35), we choose the four-dimensional phase-parameter space ($s = 1$). Thus, the four dimensions are sky position (right ascension α and declination δ), the frequency f, and the first spin-down parameter $f^{(1)}$. For demonstration purposes, consider an exemplary continuous gravitational-wave signal with the phase parameters $f_\mathrm{s} = 100.0\,\mathrm{Hz}$, $\alpha_\mathrm{s} = 2.0\,\mathrm{rad}$, $\delta_\mathrm{s} = -1.0\,\mathrm{rad}$ and $f_\mathrm{s}^{(1)} = -10^{-10}\,\mathrm{Hz/s}$.

In this illustration, assume that we have a bank of templates available covering the whole sky, the entire Doppler frequency band [11], $f_\mathrm{s} \pm f_\mathrm{s} \times 10^{-4}$, and for the spin-down value of $f^{(1)} = -10^{-11}\,\mathrm{Hz/s}$. The attentive reader will notice that the signal's spin-down value is not covered by this template value, but mismatched by an order of magnitude. This choice will demonstrate that due to the parameter-space correlations the signal is still expected to be detected in such a search, producing a detection-statistic maximum-structure which is predicted by the global-correlation equations.

The global-correlation equations only for $m \leq 2$ have to be considered in the present example, because contributions to $|\mathcal{X}|$ in (30) from terms beyond second order are negligible, as will be shown later in Section IV D. There, the neglected third-order term in Equation (30) is estimated and found to be irrelevant, in the case of the signal investigated here, and for observation times T approximately less than 61 hours.

For the case of $m \leq 2$ the integral (30) can be obtained analytically as follows

$$\begin{aligned}\mathcal{X} &\approx \frac{\mathrm{e}^{i\Delta u_0}}{T}\int_{-T/2}^{T/2}\mathrm{e}^{i(\Delta u_1\, t+\Delta u_2\, t^2)}\,\mathrm{d}t \\ &= \frac{\sqrt{\pi}}{2T\sqrt{\Delta u_2}}\,\exp\left[i\left(\Delta u_0 - \frac{{\Delta u_1}^2}{4\Delta u_2} + \frac{\pi}{4}\right)\right]\left\{\mathrm{erf}\left[\frac{(\Delta u_1 + \Delta u_2 T)\mathrm{e}^{-i\pi/4}}{2\sqrt{\Delta u_2}}\right] - \mathrm{erf}\left[\frac{(\Delta u_1 - \Delta u_2 T)\mathrm{e}^{-i\pi/4}}{2\sqrt{\Delta u_2}}\right]\right\},\end{aligned} \tag{38}$$

where the error function $\mathrm{erf}(x)$ is defined by

$$\mathrm{erf}(x) \equiv \frac{2}{\sqrt{\pi}}\int_0^x \mathrm{e}^{-t^2}\mathrm{d}t. \tag{39}$$

Figure 2 shows $|\mathcal{X}|$ given by Equation (38) as a function of the dimensionless parameters $\Delta u_1 T$ and $\Delta u_2 T^2$. This figure visualizes the fact that when one moves away in parameter space from the global-correlation hypersurfaces at $\Delta u_m = 0$ to increasing non-zero values of Δu_m, the detection-statistic amplitude $|\mathcal{X}|$ decreases rapidly from its maximum of one towards zero, as is shown in Figure 2.

As mentioned earlier, the two equations from the family of global-correlation equations (35) to be considered for the example signal studied here are:

$$f + f\,\boldsymbol{\xi}^{(1)}\cdot\mathbf{n} + f^{(1)}\,\boldsymbol{\xi}\cdot\mathbf{n} = K_1, \tag{40a}$$
$$f^{(1)} + f\,\boldsymbol{\xi}^{(2)}\cdot\mathbf{n} + 2f^{(1)}\,\boldsymbol{\xi}^{(1)}\cdot\mathbf{n} = K_2, \tag{40b}$$

where in this case the constants $K_{1,2}$ are obtained from the signal's phase parameters $(f_\mathrm{s}, f_\mathrm{s}^{(1)}, \mathbf{n}_\mathrm{s})$ as

$$K_1 = f_\mathrm{s} + f_\mathrm{s}\,\boldsymbol{\xi}^{(1)}\cdot\mathbf{n}_\mathrm{s} + f_\mathrm{s}^{(1)}\,\boldsymbol{\xi}\cdot\mathbf{n}_\mathrm{s}, \tag{41a}$$
$$K_2 = f_\mathrm{s}^{(1)} + f_\mathrm{s}\,\boldsymbol{\xi}^{(2)}\cdot\mathbf{n}_\mathrm{s} + 2f_\mathrm{s}^{(1)}\,\boldsymbol{\xi}^{(1)}\cdot\mathbf{n}_\mathrm{s}. \tag{41b}$$

Figure 3 presents the visualization of the hypersurfaces $\mathcal{H}_1$ and $\mathcal{H}_2$ described by Equations (40a) and (40b) for the given CW signal. As described in Section IV B, when choosing $s = 1$, then we have $\dim\mathcal{H}_1 = \dim\mathcal{H}_2 = 3$.

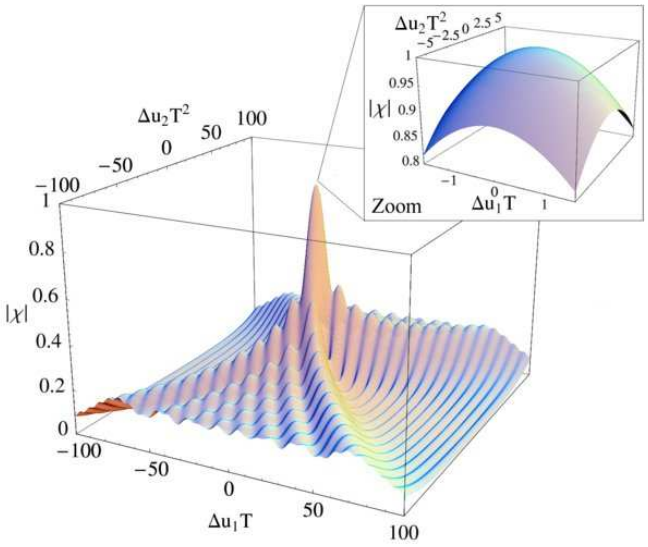

FIG. 2: (Color online) Illustration of the simplified detection-statistic amplitude $|\mathcal{X}|$ for $m \leq 2$, given by Equation (38), as a function of the dimensionless parameters $\Delta u_1 T$ and $\Delta u_2 T^2$.

In Figure 3 the subspace $\{f, \mathbf{n}\}$ is shown at the fixed target spin-down of $f^{(1)} = -10^{-11}\,\mathrm{Hz/s}$. The hypersurface described by Equation (40a) for the fixed $f^{(1)}$ is depicted three-dimensionally in Figure 3(a). The 3D plot of Figure 3(b) shows the hypersurface defined by Equation (40b) for the same signal and same template values. Finally, Figure 3(c) combines Figures 3(a) and 3(b) showing both hypersurfaces and illustrating their intersection. Along this intersection curve of both hypersurfaces, $|\mathcal{X}|$ (and so $\mathcal{F}^\star$) is expected to be maximal for the CW signal examined in this example. The contour lines of constant f (and $f^{(1)}$) in the sky of both hypersurfaces are shown on the three-dimensional unit-sphere by Figure 3(d) and in a 2D Hammer-Aitoff projection by Figure 3(e). Here, in the sky subspace the intersection curve of $\mathcal{H}_1$ and $\mathcal{H}_2$ (corresponding to maximal detection statistic) approximately coincides with the contours of $\mathcal{H}_2$.

D. Validity estimation of the global-correlation hypersurface description

This section discusses how many hypersurfaces have to be considered in order to describe the detection-statistic maximum-structure. In other words, the question is investigated, in which region of the search parameter space and at which order m the power series (29) can be truncated to approximate the matched-filtering amplitude $|\mathcal{X}|$ better than a certain fractional loss one tolerates.

For a given order m, one can estimate the contributions from the next-order term in the matched-filtering amplitude $|\mathcal{X}|$. As was done earlier in Section IV C, here we consider again the four-dimensional parameter space $\{f, f^{(1)}, \mathbf{n}\}$ of "typical" wide-band all-sky CW searches, with $f \leq 1\,\mathrm{kHz}$, $|f^{(1)}| < f/\tau_{\min}$, and a minimum spin-down age of $\tau_{\min} = 50\,\mathrm{yrs}$.

To investigate the contribution from the first-order term in Equation (30) to $|\mathcal{X}|$, we compute the following integral ignoring terms in t with order $m > 1$,

$$\mathrm{X}_1 \equiv \frac{1}{T}\int_{-T/2}^{T/2} \mathrm{e}^{i\Delta u_1\, t}\mathrm{d}t = \frac{2\sin(\Delta u_1\, T/2)}{\Delta u_1\, T}. \qquad (42)$$

Figure 4(a) shows $|\mathrm{X}_1|$ as a function of the dimensionless parameter $\Delta u_1\, T$. As already explained earlier, $|\mathrm{X}_1|$ attains its global maximum of one, when $\Delta u_1 = 0$, which is the first order global-correlation equation. If one requires for instance $|\mathrm{X}_1| \geq 0.9$, using Equation (42) this yields the condition $|\Delta u_1|\, T \leq 1.57$. When expressing Δu_1 in terms of the original phase parameters using (19), one obtains

$$\begin{aligned} |\Delta u_1| \;\lesssim\; & 2\pi\Big[\,|\Delta f|\left(1+\xi^{(1)}\right) + 2f_{\mathrm{s}}\,\xi^{(1)} \\ & +|\Delta f^{(1)}|\xi + 2|f_{\mathrm{s}}^{(1)}|\,\xi\,\Big]. \end{aligned} \qquad (43)$$

But for typical wide-band all-sky CW searches with coherent observation times T of a day or a few days, according to Equation (43) $|\Delta u_1|\, T$ can be considerably larger than 1.57. Therefore, it is clear that the first-order term in Equation (30) contributes significantly to the matched-filtering amplitude $|\mathcal{X}|$ and obviously cannot be neglected.

Similarly, we estimate the contribution from the second-order term given that $\Delta u_1 = 0$ and by ignoring terms with $m > 2$ in Equation (30). We calculate the corresponding integral denoted by X_2 as

$$\begin{aligned} \mathrm{X}_2 \;&\equiv\; \frac{1}{T}\int_{-T/2}^{T/2} \mathrm{e}^{i\Delta u_2\, t^2}\mathrm{d}t \\ &=\; \frac{\mathrm{e}^{i\pi/4}\sqrt{\pi}}{\sqrt{\Delta u_2\, T^2}}\,\mathrm{erf}\left[\frac{\mathrm{e}^{-i\pi/4}}{2}\sqrt{\Delta u_2\, T^2}\right]. \end{aligned} \qquad (44)$$

In Figure 4(b), $|\mathrm{X}_2|$ is shown as a function of $\Delta u_2\, T^2$. Obviously, $|\mathrm{X}_2|$ attains the maximum of one at the second order global-correlation hypersurface, which is described by $\Delta u_2 = 0$. One finds that $|\mathrm{X}_2| \geq 0.9$ as long as $|\Delta u_2|\, T^2 \leq 6.11$. Reexpressing Δu_2 in the original phase parameters yields

$$|\Delta u_2| \lesssim 2\pi\left[f_{\mathrm{s}}\xi^{(2)} + |\Delta f^{(1)}|\left(\frac{1}{2}+\xi^{(1)}\right) + 2|f_{\mathrm{s}}^{(1)}|\xi^{(1)}\right]. \qquad (45)$$

But according to Equation (45) for typical wideband all-sky CW searches with coherent observation times T of a day or a few days, $|\Delta u_2|\, T$ can take values considerably larger than 6.11. Therefore, the second-order term in Equation (30) also contributes significantly to the matched-filtering amplitude $|\mathcal{X}|$ and cannot be neglected.

Continuing this scheme to the next order in t, the contribution from the third-order term in Equation (30) is

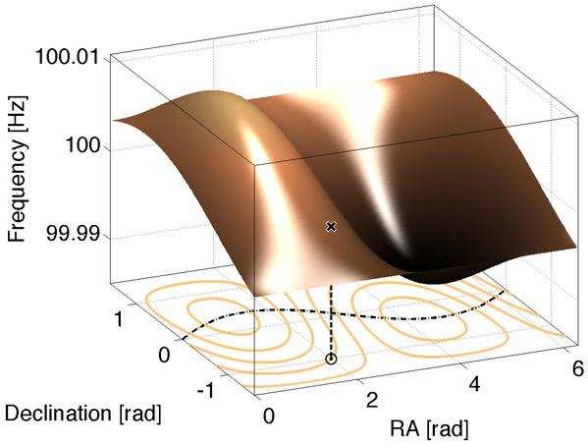

(a)Global-correlation hypersurface $\mathcal{H}_1$ and contour lines of constant frequency shown in the sky.

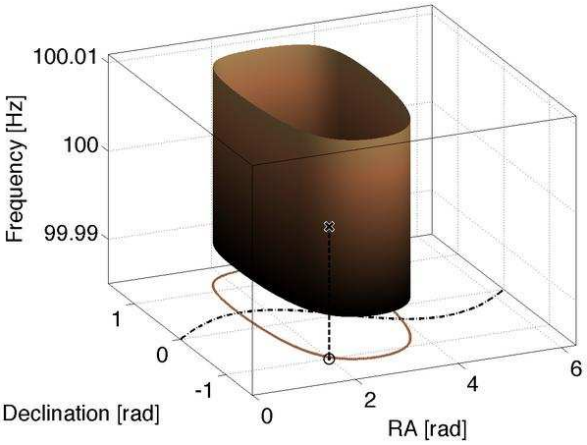

(b)Global-correlation hypersurface for $\mathcal{H}_2$ and contour lines of constant frequency shown in the sky (all close to each other).

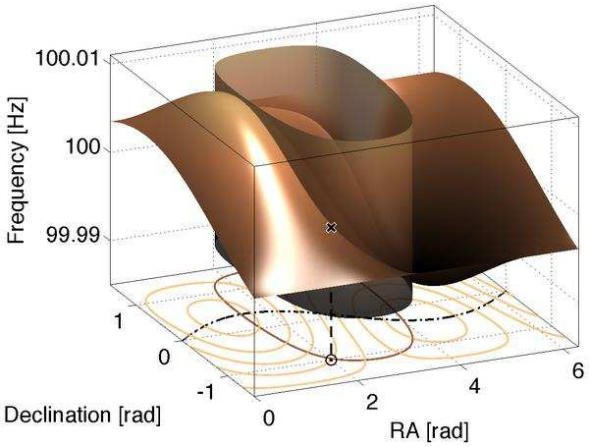

(c)Superposition of global-correlation hypersurfaces $\mathcal{H}_{1,2}$, and their frequency contour lines in the sky.

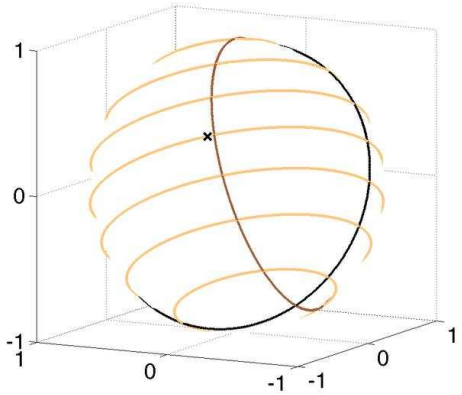

(d)Unit sphere with contour lines (circles) of global-correlation hypersurfaces $\mathcal{H}_{1,2}$.

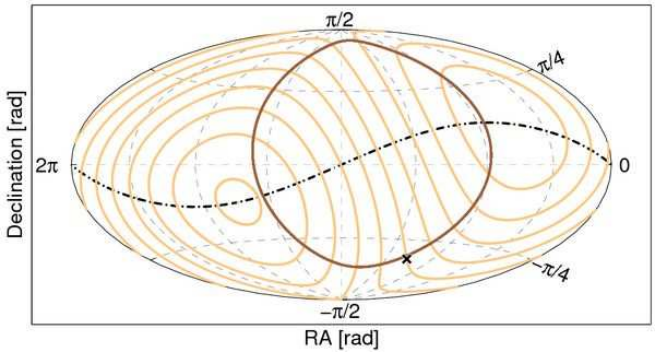

(e)Hammer-Aitoff sky projection showing the contour lines (circles) of global-correlation hypersurfaces $\mathcal{H}_{1,2}$.

FIG. 3: (Color online) The global-correlation hypersurfaces $\mathcal{H}_1$ ($\Delta u_1 = 0$) and $\mathcal{H}_2$ ($\Delta u_2 = 0$) for a given CW signal shown in the three-dimensional subspace $\{f, \mathbf{n}\}$ at the fixed target spin-down of $f^{(1)} = -10^{-11}$ Hz/s. Each plot refers to GPS time 793555944 s. The phase parameters of the signal are $\alpha_S = 2.0$ rad, $\delta_S = -1.0$ rad, $f_S = 100.0$ Hz, $f_S^{(1)} = -10^{-10}$Hz/s, as indicated by the black cross (black circle) in the subspace $\{f, \mathbf{n}\}$ (in the sky plane). In (c) the superposition of (a) and (b) illustrates the locations of expected maximum detection statistic along the intersection curve of both hypersurfaces. In each plot the light solid contour lines in the sky of constant f (and $f^{(1)}$) are of $\mathcal{H}_1$, the dark solid contour lines are the ones of $\mathcal{H}_2$. These contours of both hypersurfaces, shown in a Hammer-Aitoff projection in (e), actually describe circles on the three-dimensional unit sphere as is visualized by (d). In the sky subspace of this example, the intersection curve approximately coincides with the contours of $\mathcal{H}_2$, and due to the mismatch in spin-down the intersection curve does not pass through the signal's true sky-location. The black dotted-dashed curve represents the ecliptic.

considered. Given $\Delta u_1 = 0$ and $\Delta u_2 = 0$, we estimate the contribution from the third-order term (with $m = 3$) by evaluating:

$$\begin{aligned} \mathrm{X}_3 &\equiv \frac{1}{T}\int_{-T/2}^{T/2} \mathrm{e}^{i\,\Delta u_3\, t^3}\mathrm{d}t \\ &= \frac{\mathrm{e}^{i\pi/6}}{3\,(\Delta u_3 T^3)^{1/3}}\left[2\,\Gamma\left(\frac{1}{3}\right) - \Gamma\left(\frac{1}{3}, \frac{i}{8}\,\Delta u_3\, T^3\right)\right. \\ &\quad \left. -\Gamma\left(\frac{1}{3}, -\frac{i}{8}\,\Delta u_3\, T^3\right)\right], \end{aligned} \tag{46}$$

where the gamma function $\Gamma(x)$ and the upper incomplete gamma function $\Gamma(a, x)$ are defined by

$$\Gamma(x) \equiv \int_0^\infty t^{x-1}\,\mathrm{e}^{-t}\,\mathrm{d}t, \tag{47}$$

$$\Gamma(a, x) \equiv \int_x^\infty t^{a-1}\,\mathrm{e}^{-t}\,\mathrm{d}t. \tag{48}$$

As can also be seen from Figure 4(c), where $\Delta u_3\, T^3$ is plotted against $|\mathrm{X}_3|$, requiring $|\mathrm{X}_3| \geq 0.9$ leads to the condition $|\Delta u_3|\, T^3 \leq 9.79$. By rewriting Δu_3 using again the original phase parameters according to (19), one obtains

$$|\Delta u_3| \lesssim 2\pi\left(\frac{f_\mathrm{S}}{3}\,\xi^{\,(3)} + |f_\mathrm{S}^{(1)}|\xi^{\,(2)}\right). \tag{49}$$

By approximating

$$\xi^{\,(3)} \approx \Omega_\mathrm{orb}^2\,\frac{v_\mathrm{orb}}{c} \qquad \text{and} \qquad \xi^{\,(2)} \approx \Omega_\mathrm{orb}\,\frac{v_\mathrm{orb}}{c}, \tag{50}$$

a condition is obtained regarding the observation time T for which the contribution to $|\mathcal{X}|$ from the third-order term in Equation (30) is negligible:

$$T \lesssim \left[\frac{9.79\,c}{2\pi\,\Omega_\mathrm{orb}\,v_\mathrm{orb}}\left(\frac{f_\mathrm{S}}{3}\,\Omega_\mathrm{orb} + |f_\mathrm{S}^{(1)}|\right)^{-1}\right]^{1/3}. \tag{51}$$

In the example presented in Section IV C, a signal is considered with $f_\mathrm{S} = 100.0\,\mathrm{Hz}$ and $f_\mathrm{S}^{(1)} = 10^{-10}\,\mathrm{Hz/s}$. In this case, according to Equation (51) the third order can be neglected for observation times $T \lesssim 61\,\mathrm{h}$. For a similar signal and search, but for instance at $f_\mathrm{S} = 1000.0\,\mathrm{Hz}$ the third-order term is expected to be non-significant only for observation times $T \lesssim 28\,\mathrm{h}$.

However, considering cases where the third order in t is non-negligible, an analogous estimation of the contribution from the fourth-order term is necessary. Therefore, we calculate X_4 as

$$\begin{aligned} \mathrm{X}_4 &\equiv \frac{1}{T}\int_{-T/2}^{T/2} \mathrm{e}^{i\,\Delta u_4\, t^4}\mathrm{d}t \\ &= \frac{2}{(-i\,\Delta u_4\, T^4)^{1/4}} \\ &\quad \times\left[4\,\Gamma\left(\frac{5}{4}\right) - \Gamma\left(\frac{1}{4}, -\frac{i}{16}\,\Delta u_4\, T^4\right)\right]. \end{aligned} \tag{52}$$

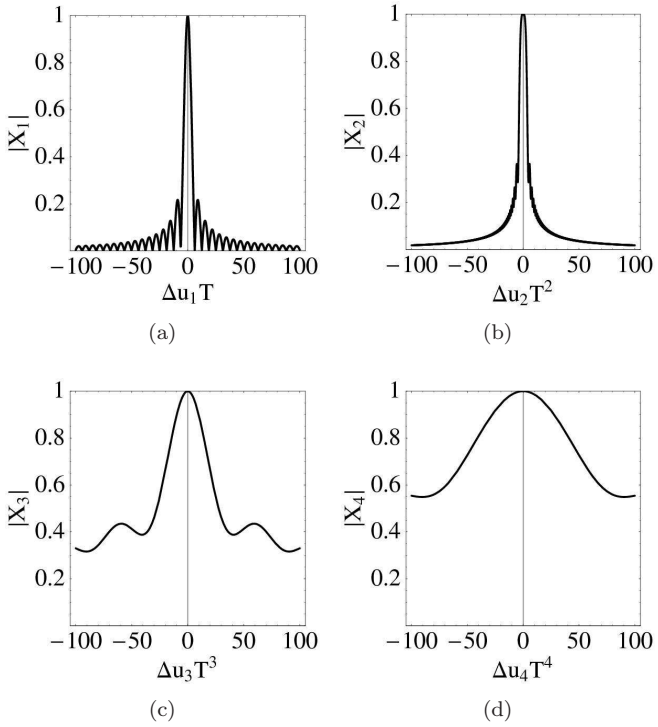

FIG. 4: Estimating the number of global-correlation hypersurfaces which contribute significantly to the detection statistic. In each plot both axes are dimensionless. Further details are given in the text.

Figure 4(d) shows $|\mathrm{X}_4|$ as a function of $\Delta u_4\, T^4$. From the condition $|\mathrm{X}_4| \geq 0.9$ follows $|\Delta u_4|\, T^4 \leq 27.78$. Using this, analogously to Equations (49) and (51), an approximate condition upon T can be found, which in the case of the present example signal yields that $|\mathrm{X}_4| \geq 0.9$ for T being approximately less than 10 days. As for the wide-band all-sky CW searches described earlier, coherent observation times are typically only of one day or a few days, this means that in practice contributions from the fourth-order term in Equation (30) to $|\mathcal{X}|$ are insignificant in such cases.

V. PREDICTIONS BY THE GLOBAL-CORRELATION EQUATIONS VERSUS FULL $\mathcal{F}$-STATISTIC

In this section the analytical predictions of the global-correlation equations (35) based on the simplified detection statistic $\mathcal{F}^\star$ are compared to the results of fully coherent searches using the detection statistic $\mathcal{F}$ in different data sets containing artificial CW signals. The computation of the full $\mathcal{F}$-statistic includes effects of amplitude modulation and involves precise calculation of the detector position with respect to the SSB using an accurate ephemeris model.

TABLE I: Amplitude and phase parameters introduced in Section III B of the two software-simulated continuous gravitational-wave signals.

Signal	A_+	$A_\times$	ψ [rad]	Φ_0 [rad]
1	1.0	0.5	1.0	2.0
2	1.0	0.0	0.0	0.0

Signal	α_S [rad]	δ_S [rad]	f_S [Hz]	$f_S^{(1)}$ [Hz/s]
1 and 2	2.0	-1.0	100.0	-10^{-10}

A. Comparison with the $\mathcal{F}$-statistic for software-simulated signals with no detector noise

Different data sets have been prepared each containing one of two different software-simulated CW signals without noise. A $\mathcal{F}$-statistic search has been conducted in each data set. The software tools used for data production as well as for data analysis are part of the LSC Algorithm Library Applications [12].

The signal parameters defining the two simulated sources are given in Table I. In both cases the phase parameters are chosen to be identical. These are also the same phase parameters of the signal generating the hypersurfaces illustrated in Figure 3. Therefore, solely based on the global-correlation equations one expects the $\mathcal{F}$-statistic to have a global large-value structure very similar to the one shown by Figure 3. To investigate the impact of the antenna pattern functions distinct amplitude parameters have been chosen here, as given by Table I. For every set of simulated data the detector position refers to the LIGO Hanford 4-km (H1) detector, and the time of reference is chosen to be global positioning system GPS time 793555944 s consistent with Figure 3.

As listed by Table II, for each data set containing the same signal different searches have been conducted, where the coherent observation time T has been varied between from 10 hours up to 2 sidereal days. In each search consisting of evaluating the $\mathcal{F}$-statistic on a grid of templates, an isotropic sky grid with equatorial spacing of 0.02 rad, spacings of $1/(2T)$ in the frequency-interval $f \in [99.8, 100.2]$ Hz and a fixed spin-down template of $f^{(1)} = -10^{-11}$ Hz/s have been employed.

First we compare the results of the searches with the prediction by the global-correlation Equation (40a) forming the hypersurface $\mathcal{H}_1$, shown in Figure 3(a). For each sky position and spin-down template-grid point where the $\mathcal{F}$-statistic search reported a candidate event with frequency $f_{\mathcal{F}}$, one can calculate the relative deviation to the predicted frequency $f_{\mathcal{F}^\star}$ obtained from Equation (40a) by $|f_{\mathcal{F}} - f_{\mathcal{F}^\star}|/f_{\mathcal{F}^\star}$. For each search the *maximum* relative deviations between predicted $f_{\mathcal{F}^\star}$ and measured $f_{\mathcal{F}}$ over the entire sky (and spin-down) are specified in Table II, and are of order 10^{-6}. The corresponding average relative deviations are typically even one order of magnitude smaller. As in the simplified phase model (17) the Earth's spinning component has been neglected, here the observed frequency-deviations are consistent with the fact that the relative corrections to the frequency modulation originating from the Earth's spinning velocity are of magnitude $v_{\text{spin}}/c \approx 10^{-6}$.

TABLE II: Comparison of predictions by the global-correlation equations based the simplified detection statistic $\mathcal{F}^\star$ with the fully coherent $\mathcal{F}$-statistic search results using data sets containing software-simulated continuous gravitational-wave signals. The search labels, listed in the first column, containing the number 1 (number 2) refer to data sets containing only Signal 1 (Signal 2), whereas labels with different letters correspond to different observation times, as can be seen from the second column. From the obtained results the *maximum* relative deviations from the predicted frequencies are specified in the third column.

Search label	Coherent observation time T	Maximum deviation $\lvert f_{\mathcal{F}} - f_{\mathcal{F}^\star}\rvert / f_{\mathcal{F}^\star}$
A1	10 hours	2.5×10^{-6}
B1	1 sidereal day	2.2×10^{-6}
C1	30 hours	2.0×10^{-6}
D1	2 sidereal days	3.2×10^{-6}
A2	10 hours	2.6×10^{-6}
B2	1 sidereal day	2.4×10^{-6}
C2	30 hours	2.3×10^{-6}
D2	2 sidereal days	3.5×10^{-6}

Finally, Figure 5 presents the results of each $\mathcal{F}$-statistic search projected on the sky. As we are only interested in the loudest $\mathcal{F}$-statistic values, only strong candidate events from the ones reported in the different searches A1,B1,C1 and D1 above a threshold of $2\mathcal{F} \geq 2000$ are shown, and for the searches A2, B2, C2 and D2 a threshold of $2\mathcal{F} \geq 1250$ is set. These thresholds were chosen to reduce the data volume to process and are based the expected global maximum values of $2\mathcal{F}$. These thresholds guarantee that candidate events with $\mathcal{F}$-statistic values at least larger than $\approx 15\%$ of the global maximum are retained in each search. This thresholding is justified because comparing candidate events with very small detection-statistic values to the global maximum are not of interest in this work.

As shown earlier in Figure 3, in the two-dimensional sky projection the intersection curve of hypersurfaces $\mathcal{H}_1$ and $\mathcal{H}_2$ approximately coincides with the contours (of constant f and $f^{(1)}$) of $\mathcal{H}_2$ in the sky. Thus, the dark circle in Figure 3(e) representing the contours of hypersurface $\mathcal{H}_2$ also describes the predicted global maximum structure of the detection statistic in the sky. In fact, this prediction is actually observed in qualitatively good agreement with the $\mathcal{F}$-statistic search results shown in Figure 5. One finds that for coherent observation times less than one sidereal day (in searches A1 and A2), the locations of the predicted global maximum structure are only faintly visible in the results, because this

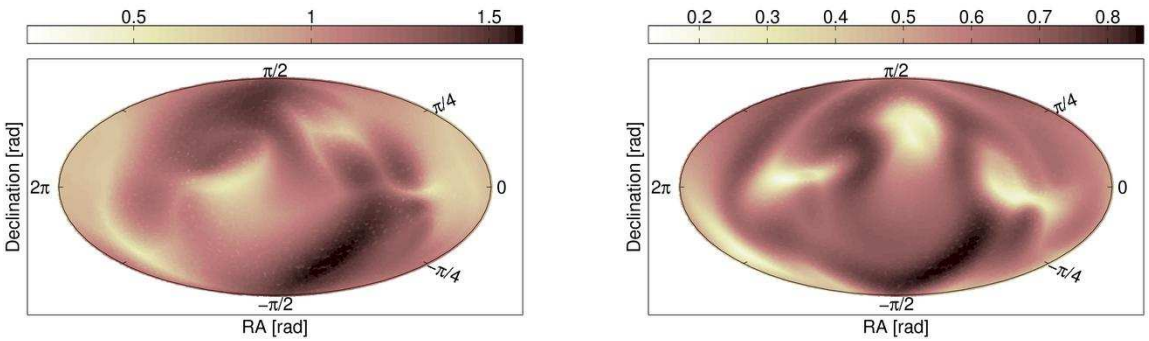

(a)Results of $\mathcal{F}$-statistic search A1 ($T = 10\,\mathrm{h}$).

(b)Results of $\mathcal{F}$-statistic search A2 ($T = 10\,\mathrm{h}$).

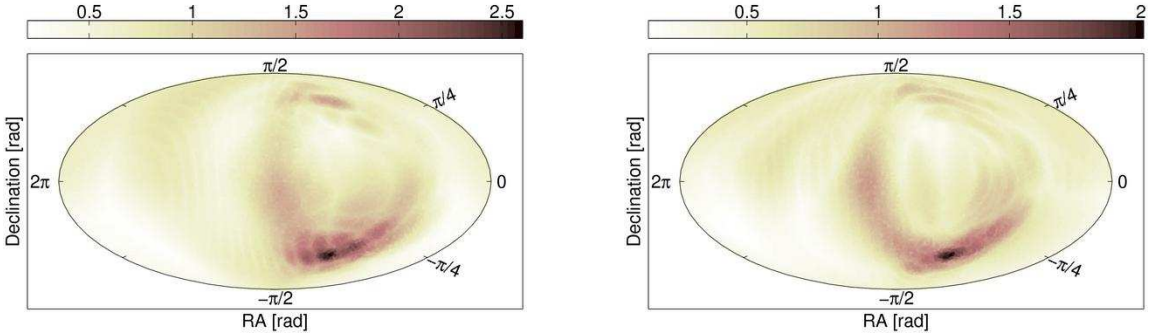

(c)Results of $\mathcal{F}$-statistic search B1 ($T = 1\,\mathrm{sd}$).

(d)Results of $\mathcal{F}$-statistic search B2 ($T = 1\,\mathrm{sd}$).

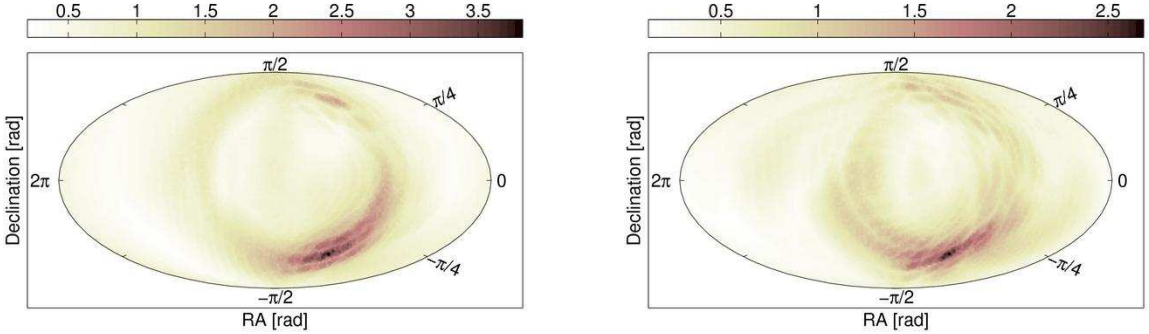

(e)Results of $\mathcal{F}$-statistic search C1 ($T = 30\,\mathrm{h}$).

(f)Results of $\mathcal{F}$-statistic search C2 ($T = 30\,\mathrm{h}$).

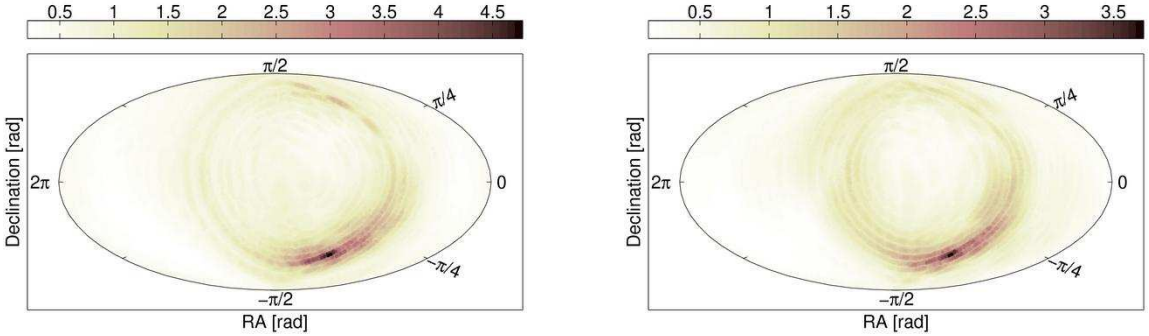

(g)Results of $\mathcal{F}$-statistic search D1 ($T = 2\,\mathrm{sd}$).

(h)Results of $\mathcal{F}$-statistic search D2 ($T = 2\,\mathrm{sd}$).

FIG. 5: Hammer-Aitoff sky projections of results from fully coherent $\mathcal{F}$-statistic searches in the data sets described by Table II. Each data set contained one of the two software-simulated CW sources defined in Table I, where both signals 1 and 2 have identical phase parameters, but different amplitude parameters. The plots of the left (right) column show candidate events registered in the different searches A1,B1,C1 and D1 (A2,B2,C2 and D2) above a threshold of $2\mathcal{F} \geq 2000$ ($2\mathcal{F} \geq 1250$). The colorbar indicates the values of $2\mathcal{F} \times 10^{-4}$. The corresponding analytical prediction by the global-correlation equations has been illustrated earlier by Figure 3(e).

feature is still hidden due to the Earth's spin component [see Figures 5(a) and (b)]. For coherent observation times beyond one period of the Earth's spinning motion, the results clearly show the locations of large $\mathcal{F}$-values as predicted [see Figures 5(c) – (h)]. As will be discussed later in Section VII, the Earth's spinning motion only varies the detection statistic within the global-correlation-equations predicted (and observed) regions.

B. Comparison with the $\mathcal{F}$-statistic for a hardware-injected signal in detector noise

For so-called "hardware injections" simulated signals are physically added into the detector control systems to produce instrumental signals that are similar to those that are expected to be produced by astrophysical sources of gravitational waves. Through magnetic coil actuators the interferometer mirrors are made to physically move as if a gravitational wave was present.

Here, we choose 30 hours of data (lying within a time span of less than 38 hours) containing a hardware injection from LIGO's fourth science run (S4) of the LIGO Livingston 4-km (L1) detector. The GPS time of reference is 795408715 s. During this data segment the hardware injection was activated 99.4% of the time. The signal's phase parameters are defined by $\alpha_{\rm S} = 3.7579\,\text{rad}$, $\delta_{\rm S} = 0.0601\,\text{rad}$, $f_{\rm S} = 575.163636\,\text{Hz}$, and $f_{\rm S}^{(1)} = -1.37 \times 10^{-13}\text{Hz/s}$, at the segment's starting time. The amplitude parameters are $A_+ = 7.48 \times 10^{-24}$, $A_\times = -7.46 \times 10^{-24}$, $\psi = -0.22\,\text{rad}$ and the initial phase is $\Phi_0 = 4.03\,\text{rad}$. In this segment of data an all-sky $\mathcal{F}$-statistic search has been carried out in the frequency interval of $f \in [575.048, 575.221]\,\text{Hz}$, and in the spin-down range $f^{(1)} \in [-1.04 \times 10^{-9}, 1.04 \times 10^{-10}]\,\text{Hz/s}$. The grid of templates employed spacings of $5.70 \times 10^{-6}\,\text{Hz}$ in f-direction, separations of $3.23 \times 10^{-10}\,\text{Hz/s}$ in $f^{(1)}$-direction, and an isotropic sky grid with equatorial spacing of 0.03 rad.

In Figure 6 the results of the actual $\mathcal{F}$-statistic search are shown and compared to the prediction by the global-correlation hypersurfaces. As the search covers a range of spin-down templates there will distinct contours of hypersurface $\mathcal{H}_2$ corresponding to each $f^{(1)}$-template. Therefore, the structure of maximum detection statistic $\mathcal{F}^\star$ is expected to be an annulus in the sky referring to the magenta region in Figure 6(b). This annulus is framed by the different contour lines of $\mathcal{H}_2$ which correspond to the minimum (dark-brown colored) and maximum (black colored) value of $f^{(1)}$ searched. Qualitatively, the large-value structure of $\mathcal{F}$ that is visible, is in good agreement with the predicted structure based on the global-correlation hypersurfaces. In Figure 6(a) the $\mathcal{F}$-statistic results only faintly reproduce the entire predicted structure because of the Earth's spinning motion. Section VII will discuss and explain analytically how the Earth's spinning motion varies the detection statistic within the regions determined by the global-correlation hypersurfaces.

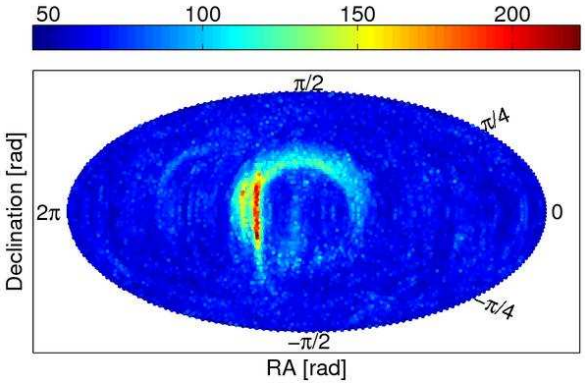

(a) Results of a coherent all-sky $\mathcal{F}$-statistic search in a data set containing a hardware-injected signal. The colorbar indicates the values of $2\mathcal{F}$.

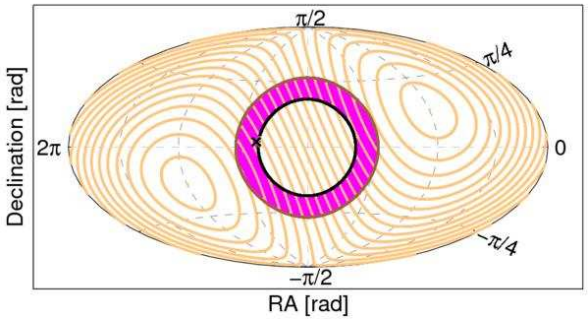

(b) Prediction of the global maximum structure of the detection-statistic based on the global-correlation hypersurfaces.

FIG. 6: Comparing the $\mathcal{F}$-statistic results (a) for a hardware-injected CW signal with the theoretical prediction (b) by the global-correlation equations. Both plots show Hammer-Aitoff projections of the sky. The sky location of the simulated signal is represented by the black cross in (b). The magenta region in (b) represents the predicted structure of maximum detection statistic $\mathcal{F}^\star$ and is observed to agree qualitatively well with the actual $\mathcal{F}$-statistic results (a) from the hardware injection in real detector data.

VI. VETOING INSTRUMENTAL NOISE ARTIFACTS

A typical feature of the data from an interferometric gravitational-wave detector are narrow-band noise artifacts, so-called "lines", which are of instrumental origin. As a consequence, the results of a search for continuous gravitational-wave sources contain instrumental artifacts that in some respects mimic CW signals. But these artifacts tend to cluster in certain regions of parameter space. For the case of *incoherent* searches as reported in [13], candidate events in such parameter-space regions were identified and discriminated. Here, we propose a similar veto method also suitable for *coherent* CW searches,

such as those found in [14]. Using the global-correlation equations found in this work we aim to identify those regions in parameter space where instrumental noise lines can imitate a real signal by producing large detection-statistic values. In such a case these candidate events could automatically be vetoed.

For simplicity we consider the same four-dimensional parameter space as used in Section IV B consisting of $\{f, f^{(1)}, \mathbf{n}\}$ and that T has a value, such that third-order contributions to $|\mathcal{X}|$ are insignificant (cf. Section IV D). Thus, the global-correlation equations of relevance are the same as in the example studied in Section IV C. These were given by Equations (40a) and (40b). It is obvious that the frequency of a stationary instrumental line is independent of the Earth's position in its orbit around the sun. This decoupling is achieved by setting $\mathbf{n}_{\mathrm{S}} = \mathbf{0}$. For a stationary instrumental line originating from the detector it also holds that $f_{\mathrm{S}}^{(1)} = 0$. In this case the constants $K_{1,2}$ in Equations (40a) and (40b) simplify to $K_1 = f_{\mathrm{s}}$ and $K_2 = 0$. Thus, the two relevant global-correlation equations are of the following form,

$$f + f\,\boldsymbol{\xi}^{(1)} \cdot \mathbf{n} + f^{(1)}\,\boldsymbol{\xi} \cdot \mathbf{n} \;=\; f_{\mathrm{s}}, \qquad \text{(53a)}$$

$$f^{(1)} + f\,\boldsymbol{\xi}^{(2)} \cdot \mathbf{n} + 2f^{(1)}\,\boldsymbol{\xi}^{(1)} \cdot \mathbf{n} \;=\; 0. \qquad \text{(53b)}$$

As stated earlier, for a given $f^{(1)}$, Equation (53a) describes a three-dimensional hypersurface in the subspace $\{f, \mathbf{n}\}$. On this hypersurface the detection statistic will attain its maximum along the intersection curve with the hypersurface described by Equation (53b). In a projection into the sky subspace this intersection curve approximately coincides with the contours (of constant f and $f^{(1)}$) of hypersurface (53b). Therefore Equation (53b) describes the region in the sky for which potential CW signals do not produce a modulation pattern that would distinguish them from an instrumental line.

Using this knowledge one can discriminate (veto) candidate events which satisfy Equation (53b). As the resolution in parameter space is finite, we formulate the following *veto condition*:

$$\left| f^{(1)} + f\,\boldsymbol{\xi}^{(2)} \cdot \mathbf{n} + 2f^{(1)}\,\boldsymbol{\xi}^{(1)} \cdot \mathbf{n} \right| < \varepsilon, \qquad \text{(54)}$$

the tolerance-parameter $\varepsilon > 0$ can be understood as

$$\varepsilon = \frac{\Delta f_{\mathrm{cell}}}{\Delta T}\, N_{\mathrm{cell}}, \qquad \text{(55)}$$

where Δf_{cell} denotes the resolution in the frequency-direction (width of cells), N_{cell} the number of cells one tolerates during a characteristic length of time ΔT.

One can visualize and calculate the volume of the region in four-dimensional parameter space which is excluded by this veto. For a given source sky position, Equation (54) is linear in f and $f^{(1)}$. Thus, for fixed sky position $\mathbf{n}$, the veto condition defines two parallel lines in the $\{f, f^{(1)}\}$ – plane. Candidate events which lie in the region between the lines are discarded (vetoed). Candidate events which lie outside this region are retained (not vetoed). The locations of these two lines in the $\{f, f^{(1)}\}$ – plane depends upon the sky position. The fractional volume excluded by the veto depends upon whether or not (as the source position varies over the sky) the excluded region between the lines lies inside or outside of the boundaries of the search, or intersects it. Alternatively, for a given value of f and $f^{(1)}$, one can calculate the portion of the sky which is excluded by the veto, depending upon the ranges of parameter space searched. The details of such a calculation for a particular search can be found in Appendix A of [14].

Figure 7 illustrates the veto method for an example noise line. Thereby, Figure 7(a) presents the results of a fully coherent matched-filtering search using the $\mathcal{F}$-statistic for a 30-hour observation time. The data set analyzed contains a detector-noise line, which is in this case a violin mode resonance of the mode cleaner mirrors of the LIGO Hanford 4-km (H1) detector. In Figure 7(b), a comparison with the theoretical prediction by the global-correlation equations given by (53a) and (53b) is made featuring a very good agreement. Thus the veto will be very efficient in excluding the parameter-space regions of largest $2\mathcal{F}$-values produced by instrumental lines.

Note that this veto excludes only the loudest candidate events (of largest $2\mathcal{F}$), but as shown in Figure 7 an instrumental line is capable of contaminating large parts of the sky due to the global correlations (depending on the search parameters). Therefore in some cases it might be necessary to increase the tolerance-parameter ε artificially to account for these effects if necessary. However, in a $\mathcal{F}$-statistic search one is interested in the strongest candidate events arising from the background level. Thus in eliminating such false instrumental-noise events the veto condition presented is very efficient as these regions are well described. This veto method as presented here is applied in the Einstein@Home search described in [14].

VII. EFFECTS OF THE DIURNAL SPINNING MOTION OF THE EARTH

By considering the Earth's spinning motion in the phase model, we here investigate the variation of the detection statistic along the predicted global maximum structure by the global-correlation hypersurfaces. In other words, given the solution $\Delta u_m = 0$, which are the the global-correlation hypersurfaces, we study how the spin component $\phi_{\mathrm{spin}}(t)$ of Equation (13) in the phase model (4) modulates the detection statistic in the locations consistent with this solution. In order to simplify this discussion, in what follows frequency time-derivatives in the spin component $\phi_{\mathrm{spin}}(t)$ are ignored to obtain

$$\phi_{\mathrm{spin}}(t) \approx 2\pi\, f\, \frac{\mathbf{r}_{\mathrm{spin}}(t) \cdot \mathbf{n}}{c}. \qquad \text{(56)}$$

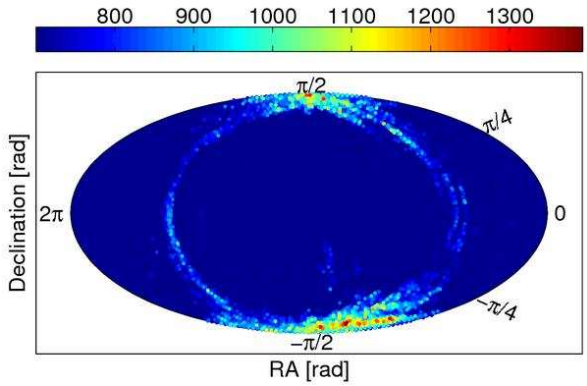

(a)Results of a coherent all-sky $\mathcal{F}$-statistic search in a data set containing an instrumental noise line. The colorbar indicates the values of $2\mathcal{F}$.

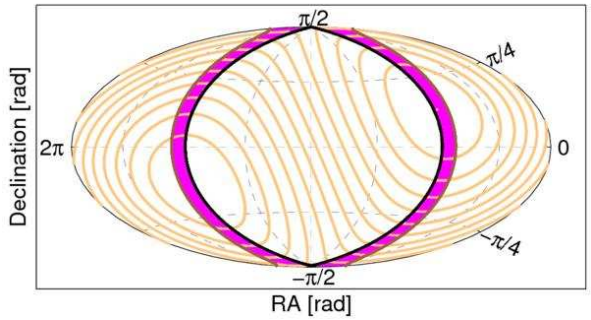

(b)Prediction of the global maximum structure of the detection statistic based on the global-correlation hypersurfaces.

FIG. 7: Comparing the results of a fully coherent matched-filtering search using the $\mathcal{F}$-statistic (a) with the theoretical prediction (b) by the global-correlation equations for a given instrumental-noise feature mimicking a real CW signal. Both plots show Hammer-Aitoff projections of the sky. The all-sky search was carried out in a 0.5 Hz frequency-band $f \in [568.0, 568.5]$ Hz and for a range of frequency time-derivatives $f^{(1)} \in [-3.63 \times 10^{-9}, 3.63 \times 10^{-10}]$ Hz/s, for an observation time of $T = 30$ h. The GPS time of reference is 795149016 s. The upper plot (a) shows all candidate events reported by the search above a detection-statistic threshold of approximately 50% of the largest $2\mathcal{F}$-value found. The frequency of the instrumental-noise line present in this data set is a resonance violin mode of the mode cleaner mirrors of the LIGO Hanford 4-km (H1) detector. The magenta region in (b) of maximum expected detection statistic agrees well with the $\mathcal{F}$-statistic results (a) from the real instrumental line.

Thus, the phase difference between the spin component of the signal $\phi^{\mathrm{S}}_{\mathrm{spin}}(t)$ and a template $\phi_{\mathrm{spin}}(t)$ is given by

$$\begin{aligned}\Delta\phi_{\mathrm{spin}}(t) &\equiv \phi^{\mathrm{S}}_{\mathrm{spin}}(t) - \phi_{\mathrm{spin}}(t)\\ &= 2\pi\,\frac{\mathbf{r}_{\mathrm{spin}}(t)}{c}\cdot(\mathbf{n}_{\mathrm{S}} f_{\mathrm{S}} - \mathbf{n} f)\\ &= \frac{\mathbf{r}_{\mathrm{spin}}(t)}{c}\cdot\Delta\mathbf{k},\end{aligned} \tag{57}$$

where we defined the vector

$$\Delta\mathbf{k} \equiv 2\pi\,(\mathbf{n}_{\mathrm{S}} f_{\mathrm{S}} - \mathbf{n} f)\,. \tag{58}$$

Taking into account $\Delta\phi_{\mathrm{spin}}(t)$ in the detection-statistic amplitude and provided that $\Delta u_m = 0$, one has to compute the following integral

$$X_{\mathrm{spin}} \equiv \frac{1}{T}\int_{-T/2}^{T/2} \mathrm{e}^{i\Delta\phi_{\mathrm{spin}}(t)}\,\mathrm{d}t\,. \tag{59}$$

For observation times T relevant to CW searches (of order days), the phase modulation due to the spinning motion of the Earth is oscillatory, because it has a period of one sidereal day $\Omega_{\mathrm{spin}} = 2\pi/1\,\mathrm{sd}$. Therefore, in order to evaluate (59) we follow a route previously taken in [5, 15], which makes use of the Jacobi–Anger identity:

$$\mathrm{e}^{iz\cos\theta} = \sum_{n=-\infty}^{\infty} i^n J_n(z)\,\mathrm{e}^{in\theta}, \tag{60}$$

where $J_n(z)$ is the n-th Bessel function of the first kind. This identity allows to expand exponentials of trigonometric functions in the basis of their harmonics. To employ the Jacobi–Anger expansion we rewrite Equation (57) by approximating the diurnal detector motion due to the Earth's rotation to be circular,

$$\begin{aligned}\Delta\phi_{\mathrm{spin}}(t) &= \frac{R_{\mathrm{E}}}{c}\Big[\Delta k_{\parallel}\sin\lambda\\ &\quad + \Delta k_{\perp}\cos\lambda\,\cos(\phi_0 + \Omega_{\mathrm{spin}} t)\Big],\end{aligned} \tag{61}$$

where R_{E} is the radius of the Earth, λ is the latitude of the detector, $\Delta k_{\parallel}$ is the absolute value of the component of the vector $\Delta\mathbf{k}$ parallel to the rotation axis, $\Delta k_{\perp}$ is the absolute value of the component of $\Delta\mathbf{k}$ orthogonal to the rotation axis, and ϕ_0 is determined by $\Delta\mathbf{k}$ at $t = 0$. Defining

$$\Delta\phi_{\mathrm{spin},\parallel} \equiv \frac{R_{\mathrm{E}}}{c}\,\Delta k_{\parallel}\sin\lambda, \tag{62}$$

$$\Delta u_{\mathrm{spin}} \equiv \frac{R_{\mathrm{E}}}{c}\,\Delta k_{\perp}\cos\lambda, \tag{63}$$

we apply the Jacobi–Anger identity:

$$\mathrm{e}^{i\Delta\phi_{\mathrm{spin}}(t)} = \mathrm{e}^{i\Delta\phi_{\mathrm{spin},\parallel}} \sum_{n=-\infty}^{\infty} i^n\,\mathrm{e}^{in\phi_0} J_n(\Delta u_{\mathrm{spin}})\mathrm{e}^{in\Omega_{\mathrm{spin}}t}. \tag{64}$$

Substituting this expression into Equation (59) and taking the modulus, one obtains

$$|X_{\mathrm{spin}}| = \left|\sum_{n=-\infty}^{\infty} i^n\,\mathrm{e}^{in\phi_0} J_n(\Delta u_{\mathrm{spin}})\,\mathrm{sinc}\left(\frac{n\Omega_{\mathrm{spin}}T}{2}\right)\right|. \tag{65}$$

Figure 8 shows $|X_{\mathrm{spin}}|$ for the two LIGO detectors as a function of T and Δu_{spin}. It is obvious that for the ob-

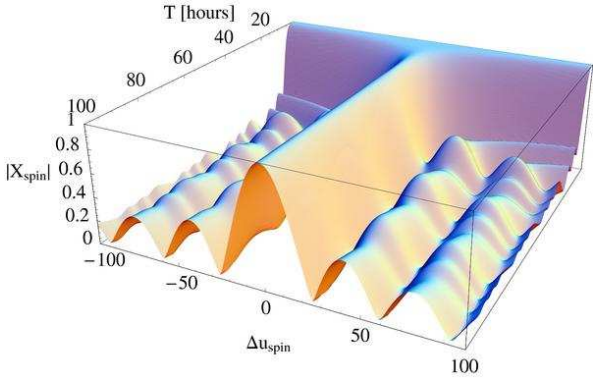

(a)LIGO Hanford detector

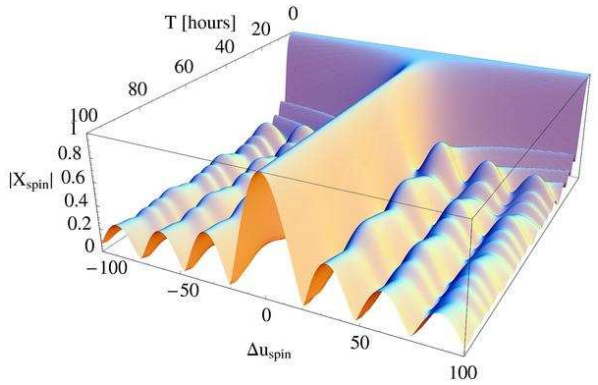

(b)LIGO Livingston detector

FIG. 8: (Color online) The simplified detection-statistic amplitude $|X_{\rm spin}|$ for phase-mismatch only in the spin component of the phase model as a function of observation time T and dimensionless parameter-mismatch $\Delta u_{\rm spin}$ as defined in Equation (63), for the two LIGO detectors. For observation times beyond $T \gtrsim 2\pi/\Omega_{\rm spin}$, a good approximation of $|X_{\rm spin}|$ is given by the dominant term $|J_0(\Delta u_{\rm spin})|$.

servation time being an integer multiple ℓ of the Earth's spin period, such that $T = 2\pi\ell/\Omega_{\rm spin}$, Equation (65) then simplifies to $|X_{\rm spin}| = |J_0(\Delta u_{\rm spin})|$, because only the term corresponding to $n = 0$ does not vanish. By inspection, we find that this is also approximately the case for all observation times of one day or longer, as can be seen from Figure 8. Therefore, we approximate $|X_{\rm spin}|$ for $T \gtrsim 2\pi/\Omega_{\rm spin}$ (which is also the regime relevant to CW searches) by

$$|X_{\rm spin}| \approx |J_0(\Delta u_{\rm spin})|. \tag{66}$$

Figure 9 illustrates $|J_0(\Delta u_{\rm spin})|$ over the entire sky for the three different cases studied previously in this work: the software-injected signal, the hardware-injected signal and the instrumental-noise line. Comparing Figure 9(a) with Figure 5, Figure 9(b) with Figure 6(a), and Figure 9(c) with Figure 7(a), one finds that the variation of the $\mathcal{F}$-statistic in the regions determined by the global-correlation hypersurfaces (locations consistent with $\Delta u_m = 0$) can in fact be recovered in Figure 9.

To illustrate better why the Earth's orbital motion determines the regions of largest detection-statistic and the Earth's spinning motion only modulates the detection-statistic within these regions, we consider the examples represented in Figure 10. There, as a basis of comparison to $|X_{\rm spin}|$ of Equation (66) we use $|\mathcal{X}|$ of Equation (38) of the orbital phase model for $m \leq 2$. As shown in Section IV D, higher orders of m are insignificant for the example cases considered. Figure 10 compares $|\mathcal{X}|$ and $|X_{\rm spin}|$ as functions of sky position for the given signal phase parameters. In the two diagrams 10(a) and (c), the sky has been sliced along α at constant declination $\delta = \delta_{\rm S}$, and for fixed values of frequency $f = f_{\rm S}$ and for simplicity also at zero spin-down offset $f_{\rm S}^{(1)} = f^{(1)}$. In the plots 10(b) and (d), the sky has been sliced along declination δ at constant right ascension $\alpha = \alpha_{\rm S}$, and for the remaining template parameters coinciding with the signal's parameters. The essential observation is that $|\mathcal{X}|$ drops off much more rapidly compared to $|X_{\rm spin}|$. Therefore, $|\mathcal{X}|$ dominantly determines the global maximum structure of the detection statistic, whereas $|X_{\rm spin}|$ only modulates the detection statistic within these regions where $|\mathcal{X}|$ is maximal.

VIII. CONCLUSIONS

The family of global-correlation hypersurfaces derived in this paper provides a approximate analytical description of the global large-value structure of the optimal detection statistic $\mathcal{F}$ in the phase-parameter space of continuous gravitational-wave searches.

For observation times longer than one sidereal day, but still much smaller compared to one year, it is the orbital motion of the Earth which generates a family of global-correlation equations. The solution to each of these equations is a different hypersurface in parameter space. The detection statistic is expected to have large values at the intersection of these hypersurfaces. In this context, the Earth's spinning motion plays a minor role, because it only varies the detection statistic within the intersection regions determined by the global-correlation hypersurfaces.

While embedding previously published results [5] in the present theory, this work leads to a substantially improved understanding of the global correlations in the optimal detection statistic.

In a comparison study with results of the $\mathcal{F}$-statistic from numerically simulated as well as from hardware-simulated signals in the presence of noise, the analytical predictions by the global-correlation equations have been qualitatively well recovered.

In addition, the global large-value structure of the detection statistic produced by stationary instrumental-noise lines mimicking astrophysical sources is also well described by the global-correlation equations. This permitted the construction of a veto method, where such false candidate events are excluded.

Moreover, reparameterization of the original phase

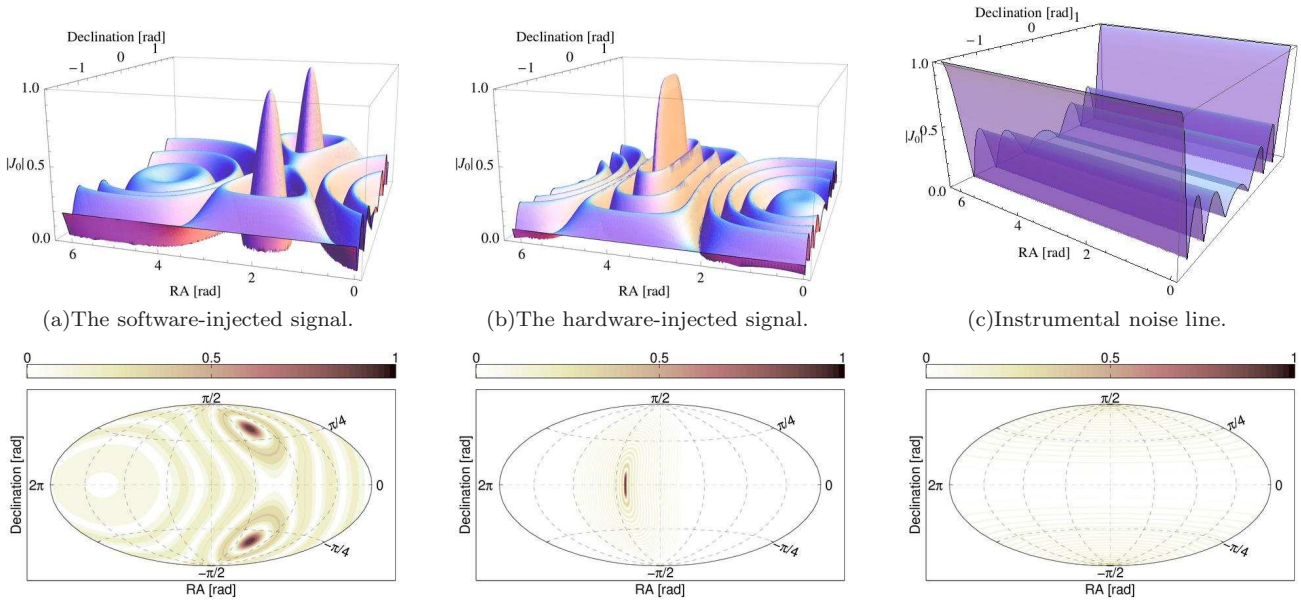

(a)The software-injected signal. (b)The hardware-injected signal. (c)Instrumental noise line.

FIG. 9: (Color online) Shown is $|X_{\text{spin}}| \approx |J_0(\Delta u_{\text{spin}})|$ over the entire sky using equatorial coordinates of right ascension α and declination δ for the three different examples studied previously in this work. The first column corresponds to the software-simulated signal [cf. Figure 5], the second column to the hardware-injected signal [cf. Figure 6(a)], and the third column to the instrumental-noise line [cf. Figure 7(a)]. In the top row, three-dimensional plots of $|J_0(\Delta u_{\text{spin}})|$ as functions of α and δ are shown, and in the bottom row two-dimensional Hammer-Aitoff projections of the sky are given illustrating the contours of $|J_0(\Delta u_{\text{spin}})|$.

parameters by the parameters u_m from the global-correlation equations offers evident advantages in solving further problems related to CW searches. For example using the u_m-parameters can help in placing templates more efficiently. As these parameters "absorb" the global correlations leading to a linear phase model, the metric in these parameters will be flat, which means independent of the parameters (cf. [16]).

Furthermore, one could implement a candidate-event coincidence scheme via reparameterizing the phase parameters of the candidate events by the u_m-parameters. In the results from a coherent search using a bank of templates, a putative signal should accumulate large detection statistic values in a very focused region in the space of u_m-parameters, because for the templates located along the contours of the global large-value structure, the parameters u_m are approximately invariant. In addition this fact gives rise to a novel type of hierarchical semi-coherent search technique for CW sources. In such a multistage scheme [9, 10] one breaks up the data set into a sequence of short data segments, of which each segment is analyzed coherently in a first stage. This is followed by an incoherent combination of the coherent results from each segment. The transformation to global-correlation parameters u_m helps classifying coincident candidate events from the first-stage coherent step before these are combined incoherently. However, in future work the efficiency of such a correlation transform scheme [17] as well as the relevance of the global correlations in the context of the template-placing problem should be investigated.

IX. ACKNOWLEDGMENTS

I am deeply grateful to Bruce Allen for his guidance and many helpful discussions. I also thank Reinhard Prix for stimulating conversations and useful comments on the manuscript. I gratefully acknowledge the support of the Max-Planck-Society and the IMPRS on Gravitational Wave Astronomy. I also acknowledge the LIGO Scientific Collaboration for the usage of data.

[1] P. Jaranowski, A. Królak, and B. F. Schutz, Phys. Rev. D **58**, 063001 (1998).
[2] B. J. Owen, Phys. Rev. D **53**, 6749 (1996).
[3] P. R. Brady, T. Creighton, C. Cutler, and B. F. Schutz, Phys. Rev. D **57**, 2101 (1998).
[4] R. Prix, Phys. Rev. D **75**, 023004 (2007).
[5] R. Prix and Y. Itoh, Class. Quantum Grav. **22**, S1003 (2005).
[6] The effects of the neutron star's proper motion in this context are discussed in [8, 18]. Assuming an extreme

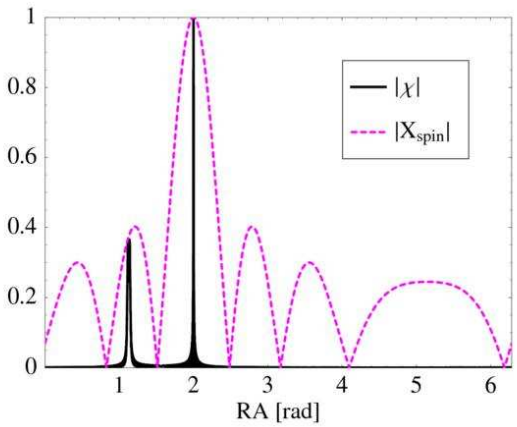

(a)The software-injected signal.

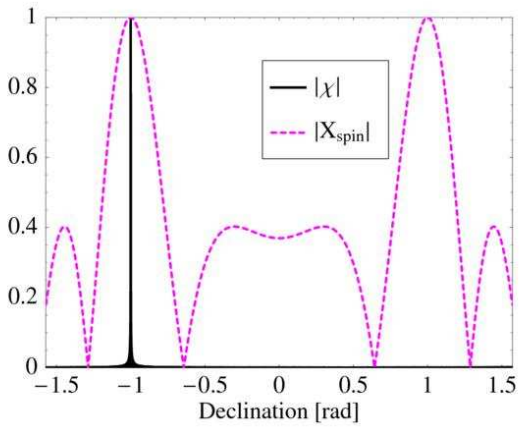

(b)The software-injected signal.

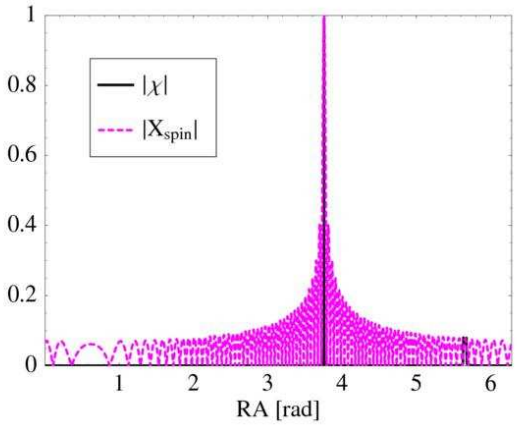

(c)The hardware-injected signal.

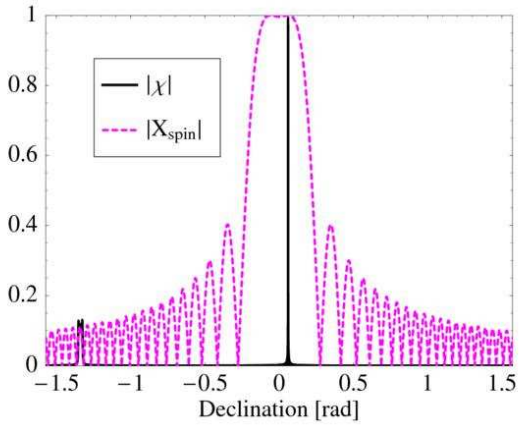

(d)The hardware-injected signal.

FIG. 10: (Color online) Comparison of $|\mathcal{X}|$ (solid curves) computed using $\Phi_{\rm orb}(t)$ and $|X_{\rm spin}|$ (dashed curves) calculated using $\phi_{\rm spin}(t)$ as functions of sky position. In (a) and (b) the signal's phase parameters correspond to the software injection of Section V A, and (c) and (d) refer to the hardware-injected signal introduced in Section V B. In (a) and (c), $|\mathcal{X}|$ and $|X_{\rm spin}|$ are shown as functions of right-ascension (RA) template-value α for the given signal-value $\alpha_{\rm S}$, while fixing the remaining template parameters to perfectly match the signal's parameters, $\delta_{\rm S} = \delta$, $f_{\rm S} = f$ and $f^{(1)}_{\rm S} = f^{(1)}$. Whereas in (b) and (d), $|\mathcal{X}|$ and $|X_{\rm spin}|$ are shown as functions of declination template-value δ, while the remaining template parameters coincide with the signal's phase parameters. One can see that $|\mathcal{X}|$ decreases much more rapidly compared to $|X_{\rm spin}|$. Therefore $|\mathcal{X}|$ dominantly determines the global maximum structure of the detection statistic.

case where the star moves with respect to the SSB at 10^3 km/s and its distance to the detector to be at 40 pc, over 120 days of observation, fitting factors (fraction of signal-to-noise ratio when using a filter not perfectly matching to a signal) greater than 99% are obtained. In addition, in this paper observation times of order a few days, much less than 120 days, are considered and therefore the proper-motion effects are neglected.

[7] P. Jaranowski and A. Królak, Living Rev. Relativity **8** (2005).

[8] P. Jaranowski and A. Królak, Phys. Rev. D **59**, 063003 (1999).

[9] B. Krishnan, A. M. Sintes, M. A. Papa, B. F. Schutz, S. Frasca, and C. Palomba, Phys. Rev. D **70**, 082001 (2004).

[10] C. Cutler, I. Gholami, and B. Krishnan, Phys. Rev. D **72**, 042004 (2005).

[11] The maximum Doppler frequency shift due to the Earth motion is given approximately by the maximum Earth's orbital velocity $v_{\rm orb}/c \approx 10^{-4}$.

[12] The LSC Algorithm Library Applications, available at `http://www.lsc-group.phys.uwm.edu/daswg/`.

[13] B. Abbott et al. (The LIGO Scientific Collaboration), Phys. Rev. D **77**, 022001 (2008).

[14] B. Abbott et al. (The LIGO Scientific Collaboration), Phys. Rev. D **79**, 022001 (2009).

[15] K. Jotania, S. R. Valluri, and S. V. Dhurandhar, Astron. Astrophys. **306**, 317 (1996).

[16] P. Astone, K. M. Borkowski, P. Jaranowski, and A. Królak, Phys. Rev. D **65**, 042003 (2002).

[17] H. J. Pletsch, *in preparation*.

[18] P. Jaranowski and A. Królak, Phys. Rev. D **61**, 062001 (2000).